# PANEL FLUTTER SIMULATION CONSIDERING TURBULENT BOUNDARY LAYER

**Atsushi Hashimoto*, Takashi Aoyama***
***Japan Aerospace Exploration Agency(JAXA)**

**Keywords**: *Aeroelasticity, Panel Flutter, Fluid-Structure Interaction, CFD*

## Abstract

*Numerical studies were carried out to investigate the effects of turbulent boundary layers on panel flutter at supersonic speeds. In this study, RANS equations are solved to take into account the turbulent boundary layer and its viscous effects. The computed flutter boundaries agree well with experimental data. Moreover, the results showed that the viscous effects were important and should be taken into account for flutter computation. Then, the boundary layer effects were investigated in the Mach number range of 1.0-2.4. We found that the boundary layer not only has a stabilizing effect but also a destabilizing effect, depending on the Mach number.*

## 1 Introduction

Panel flutter is well known as flutter of skin panel of rockets, supersonic transports, and fighters. This phenomenon is a self-excited oscillation of thin panels due to aeroelastic instability at supersonic speed. Much research on panel flutter has been conducted in the past, theoretically and experimentally, and some results are reviewed in Refs. [1] and [2]. Despite the simple geometry of a panel (e.g. a rectangular panel or shell), it is generally hard to obtain quantitative agreement of flutter boundaries between computation and experiment[3] since there are many factors affecting the boundaries, such as the effects of a turbulent boundary layer above the panel, structural damping, static-pressure differential across the panel, cavity resonance, and manufacturing imperfection. Therefore, efforts have been made to reduce these confounding effects and to measure flutter boundaries under ideal conditions. Nevertheless, those effects were not fully eliminated and it is hard to obtain quantitative agreement, especially in low supersonic regions ($M$=1.0-1.4). It is therefore necessary to understand these effects.

Fung[4] indicated that, among those effects, the turbulent boundary layer is the main reason why the computation can not predict flutter boundaries. Next, Muhlstein et. al[5] and Gaspers et. al[6] investigated the effects of the turbulent boundary layer in low-supersonic regions, using a test fixture that can control the thickness of the boundary layer above a panel. These experiments were performed so as to reduce the confounding effects mentioned above. They concluded that the turbulent boundary layer has a large stabilizing effect on flutter at low supersonic speeds and that the effect is the largest near $M$=1.2 and decreases rapidly with increasing Mach number up to $M$=1.4. Therefore, the effect was believed to appear near $M$=1.2 (low supersonic region).

Next, Dowell[7][8] computed the flutter boundaries under the experimental conditions[5], taking into account the mean flow variation at the boundary layer. He solved linear perturbation equations to obtain pressure on the panel. In addition, he neglected viscosity and employed a one-seventh power low as the mean velocity profile. Although his computation results are better than previous ones, agreement with the experimental data was not sufficient qualitatively.

Recently, computational fluid dynamics (CFD) has often been employed for fluid-structure coupled analysis. For panel flutter problems, Davis et. al[9] first analyzed transonic panel flutter and investigated shock-

wave motion on panels using CFD. Then, Selvam et al.[10] and Gordnier et al.[11] investigated limit cycle oscillation (LCO) above a flutter boundary and the viscous effects on its amplitude and frequency. However, no comparison with experimental data was made in their research. Moreover, viscous effects on flutter boundaries were not investigated.

In this study, we investigated the effects of a turbulent boundary layer on flutter boundaries by solving Reynolds averaged Navier-Stokes (RANS) equations. First, computed flutter boundaries were compared with the experimental data measured by Muhlstein et. al[5] at $M$=1.1-1.4 to validate our fluid-structure coupled analysis code, taking into account the viscous effects. Next, flutter boundaries at higher Mach numbers ($M$=1.1-2.4) were computed using the code, and were compared to those computed by inviscid flow to clarify the effects of the turbulent boundary layer.

## 2 Computational Method

### 2.1 Aerodynamic Solver

The governing aerodynamic equations are Euler or Reynolds-averaged Navier-Stokes (RANS) equations written in generalized coordinates. These equations are solved using the perfect gas relationship. In addition, the molecular viscous coefficient is computed by Sutherland's law and the Prandtl number is assumed to be constant.

In most panel flutter problems, the non-dimensional flutter frequency ($St_f=f_f\ a/U_f$) is much less than 1; they are 0.04-0.08 for $M$=1.1-1.4 in this problem. In addition, a very thin grid must be used to resolve the viscous sublayer. Therefore, an implicit time integration method should be employed to obtain a solution in practical time. In this study, LU-SGS involving the dual-time stepping method was employed for time integration. The numerical algorithm is written in delta form as;

$$\begin{aligned}
&\left(\frac{1}{J}\left(\frac{3}{2\Delta t}+\frac{1}{\Delta\tau}\right)+\frac{\partial}{\partial\xi}A+\frac{\partial}{\partial\eta}B+\frac{\partial}{\partial\zeta}C\right)\Delta Q^m \\
&=-\left[\frac{\partial}{\partial\xi}\left(E-\frac{1}{\mathrm{Re}}E_v\right)+\frac{\partial}{\partial\eta}\left(F-\frac{1}{\mathrm{Re}}F_v\right)+\frac{\partial}{\partial\zeta}\left(G-\frac{1}{\mathrm{Re}}G_v\right)\right]^m \\
&-\frac{1}{J}\frac{3Q^m-4Q^n+Q^{n-1}}{2\Delta t}+Q^m\left[\left(\frac{\xi_t}{J}\right)_\xi+\left(\frac{\eta_t}{J}\right)_\eta+\left(\frac{\zeta_t}{J}\right)_\zeta\right]^m \\
&\Delta Q^m=Q^{m+1}-Q^m
\end{aligned} \tag{1}$$

where $n$ is a physical time step number and $m$ is a subiteration number. When a sufficient subiteration number is used, second-order time accuracy is achieved in this formulation. The last term at the right-hand side computes a jacobian time derivative using the geometric conservation law (GCL).

Inviscid fluxes on the right hand side are computed by Roe's approximate Riemann solver with third-order MUSCL interpolation, whereas viscous fluxes are computed by a second-order central difference. Regarding the turbulence model, we employed mainly the Baldwin-Lomax model[12] (BL) since the nondimensional flutter frequency, $St_f$, is relatively low. We also employed the Spalart-Allmaras model[13] (SA) to see the effects of turbulence models. The BL model is a simple zero-equation model, whereas the SA model is a one-equation model including a convection term.

### 2.2 Structure Solver

The turbulent boundary layer forms a moderate pressure gradient in the streamwise direction above the panel, while the cavity pressure—the pressure under the panel—is assumed to be constant in this study. Therefore, the panel may deflect due to the static pressure differential across the panel, and its deflection can become large and nonlinear depending on the pressure differential. To avoid an unphysical large deflection, we employed the von Karman plate equations[14] that are nonlinear, large deformation plate equations considering in-plane stresses. We solved the equations by a finite difference method (FDM)[14]. A second-order central difference was employed for space derivatives, whereas Newmark's β method was employed for time integration.

### 2.3 Fluid-Structure Coupling method

To solve aerodynamics and structure dynamics simultaneously, a strong coupling method was used in which data is exchanged between the aerodynamic solver and structure solver in every step of the subiteration. This method can reduce the time lag between the two solvers (Ref. [10]).

Non-slip boundary conditions are implemented by setting the flow velocity on the panel surface equal to that of the panel surface. The deformation velocity and acceleration of the panel are transferred from the structure solver to the aerodynamic solver as boundary conditions, where acceleration is considered by setting the pressure gradient on the surface using the following equation:

$$\frac{\partial p}{\partial n} = -\rho \vec{a} \cdot \vec{n} \qquad (2)$$

where $p$ is pressure, $\rho$ is density, $\vec{a}$ is the acceleration vector, and $\vec{n}$ is unit vector normal to the surface. Additionally, we neglect the normal viscous stress in the equation because the Reynolds number is high. In this study, we employ the same size grid on the panel both for aerodynamic and structural computations to transfer the data easily between the two solvers.

The grid moves with the panel deflection. It is redistributed smoothly normal to the panel surface using algebraic equations[15], while the grid on the far field boundary is kept fixed to simplify the treatment of far field boundary conditions.

## 3 Computational Conditions

In this study, we employ the panel configuration and flow conditions of Muhlstein's experiment[5]. The panel configuration is shown in Fig. 1. The panel length-width ratio, $a/b$, is 0.5 and all sides are clamped. In addition, the boundary layer thickness above the panel, $\delta$, is defined as the 98% thickness at the middle of the panel as shown in Fig. 1. We mainly use 10% panel length thickness, $\delta/a$=0.1.

The computational domain employed in this study is shown in Fig. 2, which also shows the domain size. The upper boundary is high enough to avoid reflection of the shock wave from the leading edge of the wall. The adiabatic wall conditions are used for the lower boundary and the first-order extrapolation is used for the outflow boundary. Additionally, the free stream conditions are imposed for the other boundaries. Moreover, the distance between the inflow boundary and the panel front edge, $Lx$, is adjusted to realize the desired boundary layer thickness. In addition, the cavity pressure is assumed to be constant. In this study, we took the average pressure on the upper surface of the panel as the cavity pressure. In fact, the cavity pressure in the experiment was also controlled to minimize the differential pressure across the panel[5].

As for the grid numbers, 90, 59, and 95 points are used in the streamwise, spanwise, and normal directions, respectively, of which 20 points in the streamwise direction and 40 points in the spanwise direction are distributed on the panel.

An initial velocity is imposed on the panel at the beginning of the coupled simulation using the following distribution function:

$$v(x,y) = v_{ini} \sin^2(\pi x/a)\sin^2(\pi y/b) \qquad (3)$$

where $x$ is $0 \le x \le a$ and $y$ is $0 \le y \le b$. The coefficient, $v_{ini,}$ is $0.01c$ ($c$ = sonic speed). For the viscous cases, the flow field is computed to obtain the converged solution of the turbulent boundary layer in advance. Then, the solution is used as the initial condition of the coupled simulation, and the flutter boundaries are determined by computing several cases with changing Young modulus at a constant Mach number and mass ratio. The computed flutter boundaries are compared with experimental data using the nondimensional dynamic pressure, $\lambda$. Additionally, since the initial response is affected by the initial velocity and its distribution, the simulation is continued until the oscillation mode is converged.

## 4 Results

### 4.1 Dependency on grid and time step

In the previous study[16], we analyzed panel flutter in a laminar and turbulent boundary layer on the panel. The results show that the flutter boundaries are largely affected by the boundary layer, and there is a large difference in the flutter boundaries between the laminar and turbulent boundary layers. The laminar boundary layer has a larger stabilizing effect than the turbulent boundary layer at the same Reynolds number, $Re=10^5$, though the laminar boundary layer is thinner than the turbulent boundary layer. Thus, not only the boundary layer thickness but also the velocity profile is important to determine the flutter boundaries. Therefore, the velocity profile of the boundary layer must be computed accurately. Moreover, the time step is also important for fluid-structure coupled problems as mentioned in Ref. [10]. To compute accurate flutter boundaries of the panel in the turbulent boundary layer, dependency on grid resolution and time step is examined.

We examine here the dependency for the cases where the minimum grid sizes in the normal direction to the panel, $\Delta z$, are $5\times10^{-5}$, $2\times10^{-5}$, $1\times10^{-5}$, and $5\times10^{-6}$ and the time steps, $\Delta t$, are $1.25\times10^{-3}$, $2.5\times10^{-3}$, $5.0\times10^{-3}$, and $1.0\times10^{-2}$, where $z$ and $t$ are nondimensionalized by $a$ and $a\times c$, respectively. Here, $a$ is panel length in the streamwise direction and $c$ is sonic speed. All cases are computed under the conditions of $M=1.2$ and $\delta/a=0.1$. The boundary layer thickness $\delta$ is 98% thickness. In addition, the subiteration is used three times for each physical time step in all cases. The computed flutter boundaries are shown in Figs. 3 and 4. The flutter boundary is largely affected by the grid resolution and time step. As the time step decreases, the flutter dynamic pressure decreases. Conversely, as the grid size decreases, the flutter dynamic pressure increases. The limiting values are estimated by Richardson extrapolation[17]. Although the smallest time step and grid size are favorable, we selected $2.0\times10^{-5}$ and $2.5\times10^{-3}$ for $\Delta z$ and $\Delta t$, respectively, to keep the computational time needed within reason. The estimated errors are 6-9% in nondimensional dynamic pressure (Figs. 3 and 4) which is smaller than the variation due to the boundary layer, as described later. In addition, when the grid size is evaluated by $y^+$ (wall distance measured in viscous length scale), $y^+$ is 0.92 at the middle of the panel for $\Delta z$ of $2.0\times10^{-5}$ and is sufficiently small. When the time step is used, approximately 5,300 steps are included in a period of oscillation at $M=1.2$ and $\delta/a=0.1$. These selected grid size and time step are used for the following computation.

### 4.2 Structure model

Table 1 shows the natural frequencies of the first to fifth modes of the panel computed by the FDM, where the experimental data[6] is also shown for comparison. The corresponding mode shapes are illustrated in Fig. 5. Although errors of approximately 10% were observed in the third and fourth modes, the natural frequencies show reasonable agreement as a whole. The errors of the higher mode frequencies seem to be due to the different boundary conditions between computation and experiment. In fact, the edge condition of the panel in the experiment is not the ideal clamp condition, as mentioned in Ref. [6]. However, in this problem, the panel oscillates mainly with the first mode for the lower Mach numbers ($1<M\leq1.4$) and with the first and fifth modes for higher Mach numbers ($M>1.4$). Therefore, the effect caused by the errors is thought to be small.

### 4.3 Euler computation

Euler computation was carried out for Mach 1.1-1.4. The flutter boundaries determined by Euler computation are compared with Dowell's computation[7] and the experimental data[5] (Fig. 6). Dowell computed them using an inviscid small perturbation theory, whereas the experimental data are extrapolated values from the flutter boundaries measured at different boundary layer thicknesses. The flutter dynamic pressure obtained by the present method is lower for Mach 1.1-1.2 and rapidly increases with the Mach number. This computational result agrees well with Dowell's computation,

and agreement with experimental data is good except for $M$=1.4. The difference at $M$=1.4 seems to be due to the different panel boundary conditions mentioned in the previous section, since the component of the third natural mode is larger only at $M$=1.4 than at the other Mach numbers.

### 4.4 RANS computation

Next, RANS computation was carried out at $M$=1.2 considering the turbulent boundary layer. Here, we employed BL model for the turbulence model. Flutter dynamic pressures are computed for the boundary layer thicknesses in the range of $\delta/a$=0.03-0.11. Figure 7 compares the computation and experiment[5] flutter boundaries. As the thickness of boundary layer increases, the flutter dynamic pressure increases. The obtained results quantitatively agree well with the experimental data; the boundary layer has a stabilizing effect (i.e. increased flutter dynamic pressure) on flutter at $M$=1.2. In addition, the flutter boundary obtained by inviscid (Euler) computation is also shown at $\delta/a$=0 in Fig. 7. The inviscid flutter boundary is near the asymptotic value at $\delta/a$=0 of the flutter boundaries for $\delta/a$=0.03-0.11.

Figure 8 shows a snapshot of a fluttering panel, illustrating the deflected panel and pressure on the panel surface. The deflection is amplified in the visualization process so that the oscillation mode can be identified. The computational conditions are $M$=1.2, $\delta/a$=0.1, and $\lambda$=280. As shown in Fig. 8, the panel oscillates at almost the first mode at this Mach number. In addition, the pressure on the panel changes according to the defection. For example, at the moment shown in the figure, the surface pressure is high on the front side due to the compression waves and low in the back side due to the expansion waves.

Then, RANS computation was carried out at Mach 1.1-1.4 using BL and SA models. The results are shown in Fig. 9, where the computed boundaries are compared with Dowell's computation[7] and the experimental data[5]. Dowell computed them using an inviscid small perturbation theory based on a mean flow of turbulent boundary layer but he did not include the viscous effect. As shown in Fig. 9, the two computational results using BL and SA models agree well with the experimental data and it shows better agreement than Dowell's computation at Mach 1.4. This difference comes from the viscous effect that is neglected in Dowell's computation. In fact, Dowell's computation shows a similar feature to the inviscid computation, where the flutter dynamic pressure increases rapidly with the Mach number (Fig. 6). In the present computation, however, the flutter dynamic pressure increases slowly. As mentioned above, the present computational code accurately predicts the flutter boundaries. Moreover, the viscous effect is significantly important and should be taken into account in the analysis, otherwise the flutter boundaries can not be predicted accurately. In addition, the panel flutter problem employed in this study is recommended as a benchmark problem to validate a fluid-structure coupled code treating a turbulent flow, since the turbulent boundary layer effect on flutter can be examined directly and clearly.

The two models, BL and SA models, predict the flutter boundaries well and the difference between the two models is small as shown in Fig. 9, though the flutter boundaries of SA model show slightly higher than those of BL model. The BL model is a quasi-steady approximation of the turbulent boundary layer. The results show that the modeling is appropriate in this problem, probably because the nondimensional flutter frequency, $St_f$, is low. Therefore, we use the simple BL model hereafter.

### 4.5 Effect of turbulent boundary layer

Since the fluid-structure coupled code is well validated, the effects of the boundary layer were investigated further over a wide range of Mach numbers. We conducted the RANS computation using BL model at $\delta/a$=0.1 and $M$=1.1-2.4. Since there is no available experimental data for M≥1.5, the mass ratio for the mach number 1.4 was used for M≥1.5 as well. We also conducted inviscid computations for purposes of comparison. The computed flutter boundaries

are shown in Fig. 10. In the low-supersonic region, $M$=1.1-1.3, the flutter dynamic pressures at $\delta/a$=0.1 are much higher than those of inviscid case. Thus, flutter is stabilized by the boundary layer in this region. Then, the flutter dynamic pressure of the inviscid case increases rapidly near $M$=1.4, a feature similar to Dowell's computation[1]. On the other hand, the flutter dynamic pressure at $\delta/a$=0.1 increases more slowly than that of the inviscid case. This slow increase causes inversion of the flutter boundary in the region $M$=1.4-1.8, where flutter is destabilized by the boundary layer. Further, the flutter dynamic pressure at $\delta/a$=0.1 becomes higher than that of the inviscid case for M≥2.0.

Figure 11 shows the difference in flutter boundaries between the viscous (RANS) and inviscid (Euler) computations, and this difference is evaluated in the following equation.

$$DIFF = \frac{\lambda_{vis} - \lambda_{invis}}{\lambda_{invis}} \times 100\,(\%) \qquad (4)$$

From the figure, the difference appears mainly in the low supersonic region. At $M$=1.4-1.6, the difference is approximately 30%. Even recently, quasi-steady aerodynamic theory is commonly used especially for higher Mach numbers (e.g. M>1.5). Since the flutter boundaries computed by Euler equations are almost the same as those computed by the quasi-steady aerodynamic theory for M>1.5 (Ref. 9), this difference is thought to be the difference between the viscous computation and the quasi-steady aerodynamic theories.

The effects of a turbulent boundary layer on panel flutter were discussed by Muhlstein et al[5], Gaspers et al[6], and Dowell[7][8]. Their discussions are limited to the stabilizing effect of flutter in the low-supersonic region (1.1≤M≤1.3), since at that time the effect was thought to be the largest in this region. In fact, the effect is large in this region as shown in Fig. 11. However, it is necessary to consider a wide range of Mach numbers in order to understand the effects of the boundary layer. As shown in Fig. 10, the boundary layer has not only a stabilizing effect but also a destabilizing effect. The most important finding here is that the flutter dynamic pressure slowly increases due to the boundary layer at $M$=1.4-1.6. One possible reason for this slow increase could be an effect secondary to the local Mach number reduction. Because the flow near the panel becomes slow due to the boundary layer, the characteristics at the lower Mach numbers (1<M≤1.4) continue even at higher Mach numbers (M≥1.5).

## 5 Conclusions

We numerically investigated the effects of turbulent boundary layers on panel flutter. In this study, Reynolds-averaged Navier-Stokes (RANS) equations were solved using computational fluid dynamics (CFD) to take the turbulent boundary layer into account and von Karman plate equations were solved for the panel. First, the fluid-structure coupling code was validated. The grid resolution and time step were carefully selected before the computation. As a result, the flutter boundaries computed by RANS equations quantitatively agree well with the experimental data. Moreover, the comparison between the present and Dowell's computations showed that the viscous effect is significantly important and should be taken into account. In this study, the flutter boundaries with Baldwin-Lomax and Spalart-Allmaras models are compared and the difference between them is found to be small. In addition, the panel flutter problem used in this study is recommended as a benchmark problem to validate a fluid-structure coupled code treating a turbulent flow, since the turbulent boundary layer effect on flutter can be examined directly and clearly.

Then, the flutter boundaries in the range $M$=1.1-2.4 were computed using the code, and compared with those computed by inviscid flow in order to clarify the effects of a turbulent boundary layer. It was found that the boundary layer has not only a stabilizing effect but also a destabilizing effect, depending on the Mach number. The most important finding is that the flutter dynamic pressure increases slowly due to the boundary layer as the Mach number increases in the range $M$=1.2-1.5.

## References


[1] Dowell, E. H.,"A Review of the Aeroelastic Stability of Plate and Shells," *AIAA Journal*, Vol. 8, No. 3, 1970, pp. 385-399.

[2] Mei, C., Abdel-Motagaly, K., and Chen, R., "Review of Nonlinear Panel Flutter at Supersonic and Hypersonic Speeds," *Applied Mechanics Reviews*, Vol. 52, No. 10, 1999, pp. 321-332.

[3] Dowell, E. H., "Theoretical and Experimental Panel Flutter Studies in the Mach number Range 1.0 to 5.0," *AIAA Journal*, Vol. 3, No. 12, 1965, pp. 2292-2304.

[4] Fung, Y. C., "Some Recent Contribution to Panel Flutter Research," *AIAA Journal*, Vol. 1, No. 4, 1963, pp. 898-909.

[5] Muhlstein, L., Gaspers, P. A., and Riddle, D. W., "An Experimental Study of The Influence of The Turbulent Boundary Layer on Panel Flutter," NASA TN D-4486, 1968.

[6] Gaspers, P. A., Muhlstein, L., and Petroff, D. N., "Further Experimental Results on the Influence of The Turbulent Boundary Layer on Panel Flutter.", NASA TN D-5798, 1970.

[7] Dowell, E. H., "Generalized Aerodynamic Forces on a Flexible Plate Undergoing Transient Motion in a Shear Flow with an Application to Panel Flutter," *AIAA Journal*, Vol. 9, No. 5, 1971, pp. 834-841.

[8] Dowell, E. H., "Aerodynamic Boundary Layer Effects on Flutter and Damping of Plates," *AIAA Journal*, Vol. 10, No. 12, 1973, pp. 734-738.

[9] Davis, G. A. and Bendiksen, O. O., "Transonic Panel Flutter", AIAA paper 93-1476, 1993.

[10] Selvam, R. P., Visbal, M. R., and Morton, S. A., "Computation of Nonlinear Viscous Panel Flutter Using a Fully-Implicit Aeroelastic Solver," AIAA paper 98-1844, 1998.

[11] Gordnier, R. E. and Visbal, M. R., "Development of a Three-Dimensional Viscous Aeroelastic Solver for Nonlinear Panel Flutter," *Journal of Fluids and Structures*, Vol. 16, Issue 4, 2002, pp. 497-527.

[12] Baldwin, B. S. and Lomax, H., "Thin Layer Approximation and Algebraic Model for Separated Turbulent Flows," AIAA paper 78-257, 1978.

[13] Spalart, P. R. and Allmaras, S. R., "A One-Equation Turbulence Model for Aerodynamic Flows," AIAA paper 92-0439, 1992.

[14] Brown, J. C. and Harvey, J. M., "Large Deflection of Rectangular Plates Subjected to Uniform Lateral Pressure and Compressive Edge Loading," *Journal of Mechanical Engineering Science*, Vol. 11, No. 3, 1969, pp.305-317.

[15] Gordnier, R. E. and Visbal, M. R., "Development of a Three-Dimensional Viscous Aeroelastic Solver for Nonlinear Panel Flutter," AIAA paper 2000-2337, 2000.

[16] Hashimoto, A., Yagi, N., and Nakamura, Y., "Effects of Boundary Layer on Supersonic Panel Flutter," *Journal of the Japan Society for Aeronautical and Space Sciences*, Vol. 55, 2007, pp.159-164 (in Japanese).

[17] Roache, P. J., "Verification and Validation in Computational Science and Engineering," Hermosa Publication, 1998.


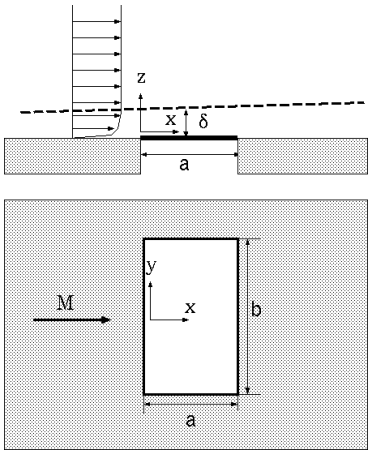


Fig. 1 Schematics of panel flutter problem.

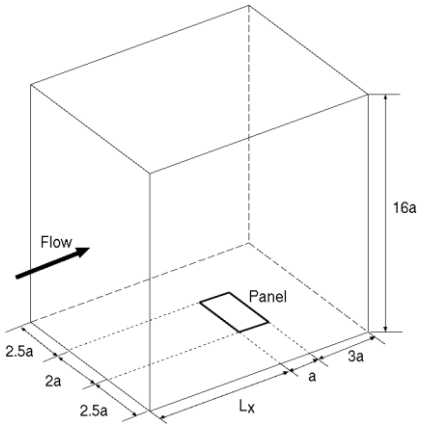


Fig. 2 Computational domain

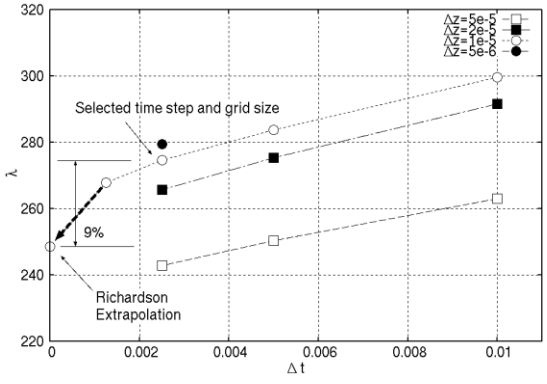


Fig. 3 Effect of time step Δt on flutter boundary.

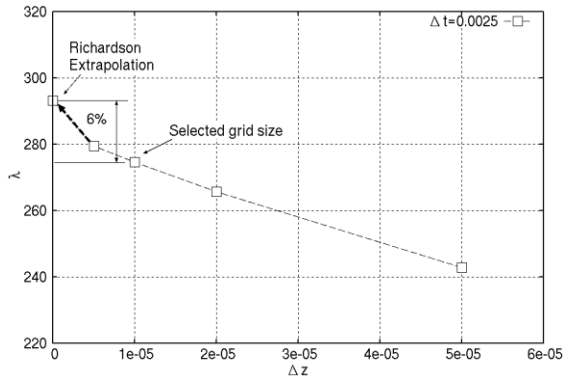


Fig. 4 Effect of grid size Δz on flutter boundary.

Table 1 Structure oscillation frequency

| Mode | 1 | 2 | 3 | 4 | 5 |
|---|---|---|---|---|---|
| FDM (Hz) | 108.1 | 138.2 | 191.7 | 267.9 | 278.4 |
| Exp (Hz) | 110.0 | 143.0 | 212.0 | 298.0 | 287.0 |
| Error (%) | 1.7 | 3.4 | 9.6 | 10.1 | 3.0 |

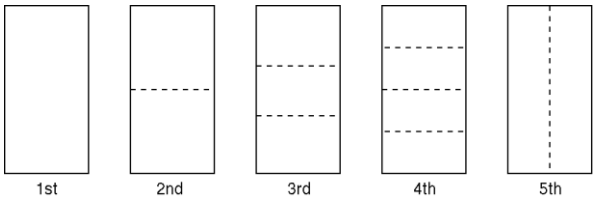


Fig. 5 Node line of natural mode.

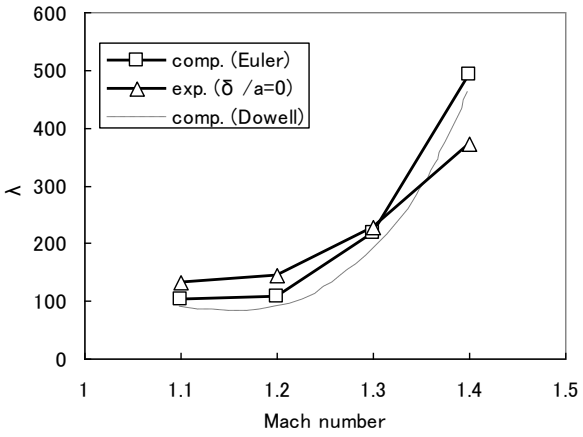


Fig. 6 Flutter boundary (inviscid case).

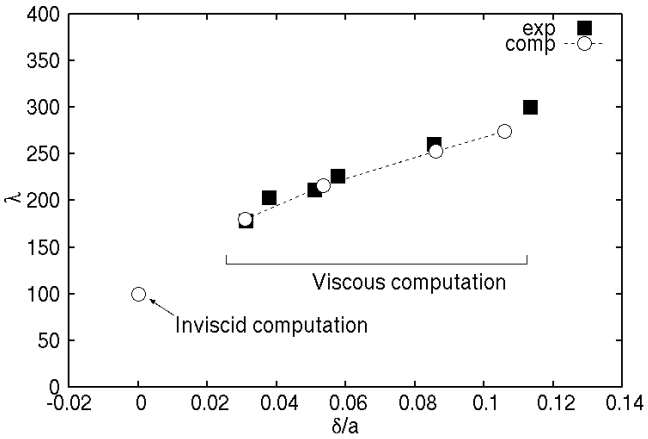


Fig. 7 Flutter boundaries vs. boundary layer thickness ($M$=1.2).

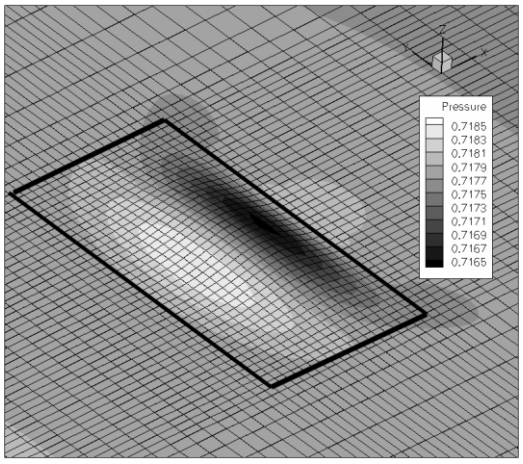


Fig. 8 Fluttering panel and surface pressure.

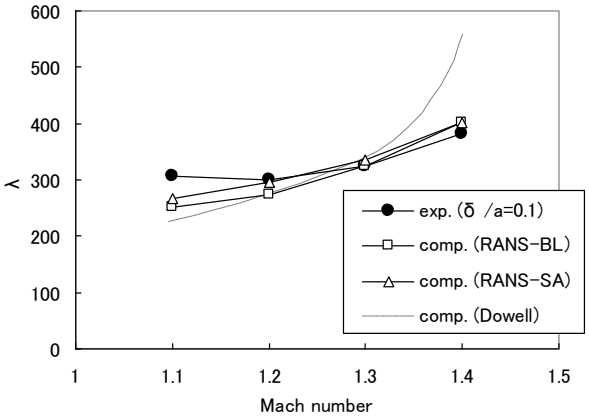


Fig. 9 Flutter boundary (viscous case).

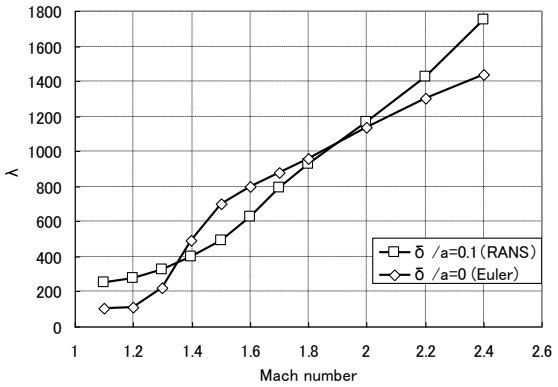


Fig. 10 Effect of turbulent boundary layer on flutter boundary.

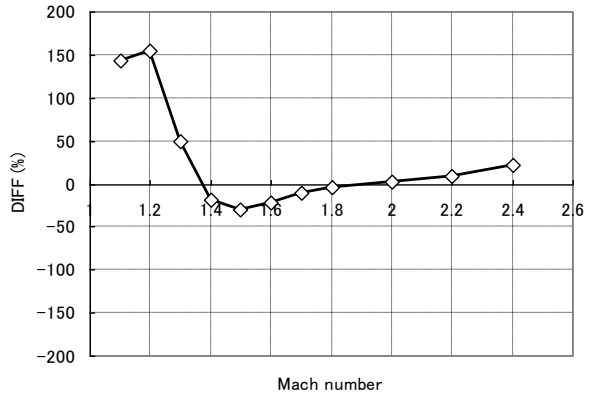


Fig. 11 Difference between inviscid and viscous computations.

## 6 Contact Author Email Address

Atsushi Hashimoto
ahashi@chofu.jaxa.jp

## Copyright Statement

The authors confirm that they, and/or their company or organization, hold copyright on all of the original material included in this paper. The authors also confirm that they have obtained permission, from the copyright holder of any third party material included in this paper, to publish it as part of their paper. The authors confirm that they give permission, or have obtained permission from the copyright holder of this paper, for the publication and distribution of this paper as part of the ICAS2010 proceedings or as individual off-prints from the proceedings.